ACS NANO
Cite This: ACS Nano XXXX, XXX, XXX–XXX
www.acsnano.org

ARTICLE

Harnessing Heat Beyond 200 °C from Unconcentrated Sunlight with Nonevacuated Transparent Aerogels

Lin Zhao, Bikram Bhatia, Sungwoo Yang,† Elise Strobach, Lee A. Weinstein, Thomas A. Cooper,‡ Gang Chen,* and Evelyn N. Wang*

Department of Mechanical Engineering, Massachusetts Institute of Technology, 77 Massachusetts Avenue, Cambridge, Massachusetts 02139, United States

Supporting Information

ABSTRACT: Heat at intermediate temperatures (120–220 °C) is in significant demand in both industrial and domestic sectors for applications such as water and space heating, steam generation, sterilization, and other industrial processes. Harnessing heat from solar energy at these temperatures, however, requires costly optical and mechanical components to concentrate the dilute solar flux and suppress heat losses. Thus, achieving high temperatures under unconcentrated sunlight remains a technological challenge as well as an opportunity for utilizing solar thermal energy. In this work, we demonstrate a solar receiver capable of reaching over 265 °C under ambient conditions without optical concentration. The high temperatures are achieved by leveraging an artificial greenhouse effect within an optimized monolithic silica aerogel to reduce heat losses while maintaining high solar transparency. This study demonstrates a viable path to promote cost-effective solar thermal energy at intermediate temperatures.

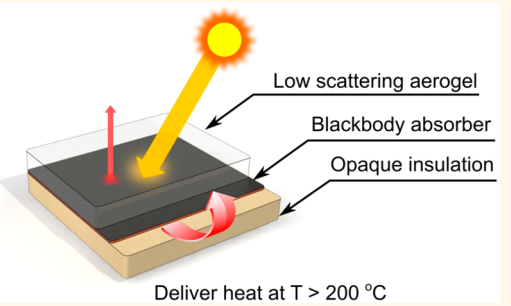

KEYWORDS: *solar thermal conversion, transparent aerogel, artificial greenhouse effect, light scattering, radiative transfer*

The greenhouse effect in the Earth's atmosphere provides the warmth essential for the survival of our ecosystem. Unfortunately, increasing human activities such as burning fossil fuels have intensified this natural greenhouse effect, leading to global warming and climate change.[1] While a temperature rise on Earth can be detrimental, a higher temperature heat source implies a higher potential for energy utilization in a heat engine when considering the Carnot efficiency. Therefore, it is possible to take advantage of this same greenhouse effect in engineering designs to boost the efficiency of terrestrial energy conversion processes such as in solar-thermal systems.[2] Thermal energy at intermediate temperatures (120–220 °C) is in particularly high demand, with more than 627 TWh of energy consumed annually in the US,[3] which is larger than the total US annual electricity generation from all renewable sources in 2016 (~599 TWh).[4] To supply heat at intermediate temperatures from the sun, state-of-the-art solar-thermal approaches, however, rely on costly optical concentrators, selective surfaces, and vacuum enclosures to effectively capture sunlight in this temperature range (120–220 °C).[5,6] Here we demonstrate a simple low-cost solar receiver capable of reaching over 265 °C under unconcentrated solar flux (1 kW/m^2) using a low-scattering, highly transparent aerogel as the artificial greenhouse medium. Much like the natural greenhouse effect, this aerogel transmits sunlight but traps heat by blocking thermal emission. The receiver requires no selective surface or vacuum enclosure and can operate at ambient conditions. The ability to supply heat with solar energy at the desired intermediate temperatures addresses the significant needs in industry and mitigates fossil fuel consumption. Our study demonstrates the feasibility of using an engineered greenhouse cavity to capture sunlight effectively and provides a viable path for leveraging the greenhouse effect to reduce greenhouse gas emissions.

Most current solar thermal technologies utilize optical concentrators to focus the dilute solar flux to generate intermediate-temperature heat from the sun. Such optical devices are expensive and require diurnal tracking of the sun.[7] While nonconcentrating systems can reach temperatures up to 250 °C by using spectrally selective surfaces as well as vacuum enclosures to suppress parasitic heat losses,[8−12] maintaining the vacuum and the radiative properties of spectrally selective surfaces over the system lifetime is challenging. Recently, solar absorbers based on plasmonic nanoparticles and 2-D materials

Received: April 17, 2019
Accepted: June 7, 2019
Published: June 7, 2019

DOI: 10.1021/acsnano.9b02976
ACS Nano XXXX, XXX, XXX–XXX

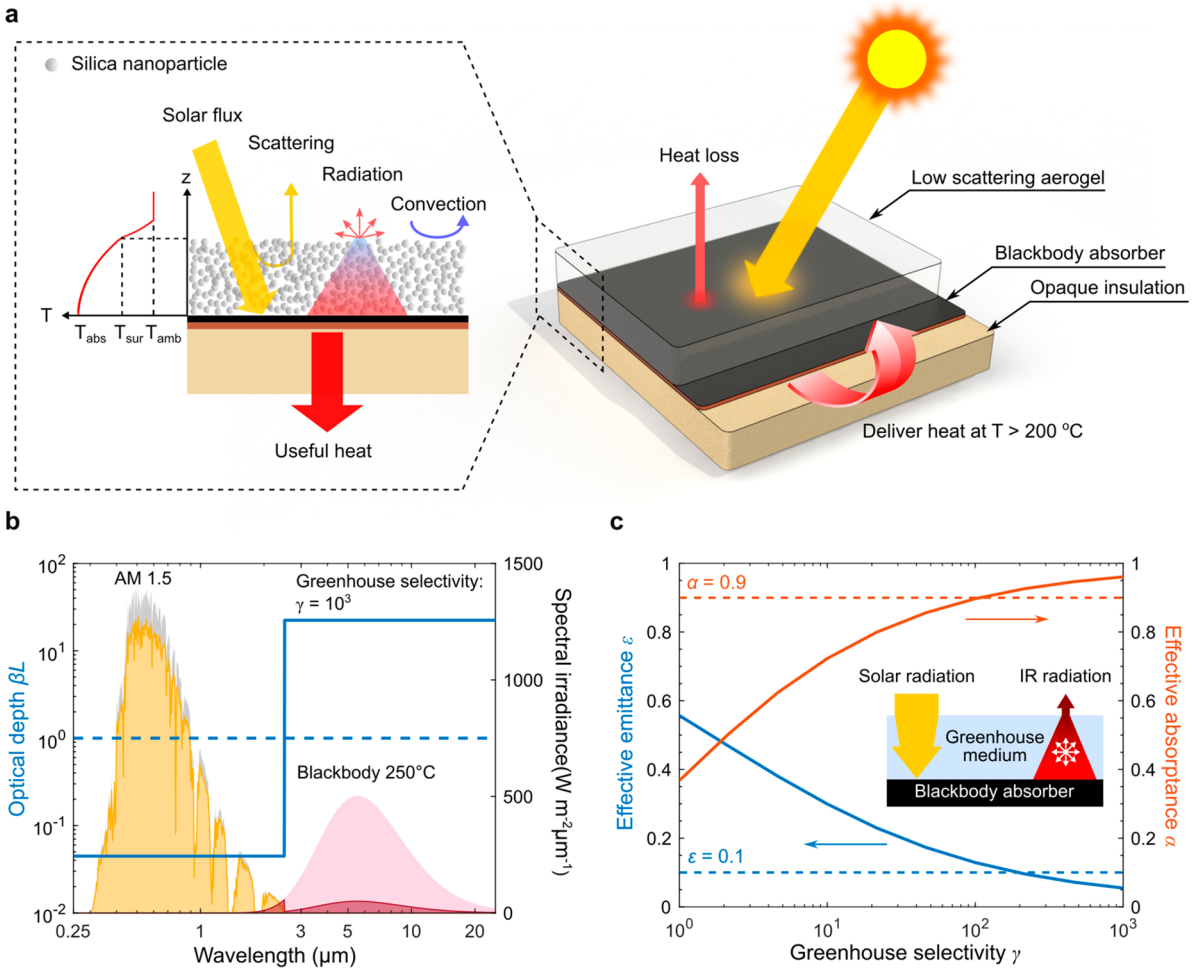

Figure 1. Harvesting unconcentrated sunlight using low-scattering aerogels as a greenhouse medium. (a) Similar to the natural greenhouse effect, the aerogel allows sunlight to transmit through but blocks thermal radiation from the blackbody absorber by strong infrared (IR) absorption. (b) Ideal optical properties of a greenhouse medium (blue solid line) with higher optical depth (*e.g.*, 1000×) in the thermal band than that in the solar band. The dashed blue line represents a nongreenhouse medium. The yellow filled area indicates the transmitted solar radiation (gray area: AM 1.5). The red filled area indicates the reduced thermal emission from the blackbody absorber (pink area: blackbody at 250 °C). (c) Effective absorptance α (red) and emittance ε (blue) of a greenhouse enhanced blackbody absorber as a function of its greenhouse selectivity. The medium thickness L is chosen such that the average (geometric mean) optical depth is fixed at unity for fair comparison: $\sqrt{\beta_{thermal}\beta_{solar}}L = 1$. Dashed lines show the typical performance of conventional spectrally selective surfaces. Inset: schematic of a greenhouse enhanced blackbody absorber.

have shown very promising results in the field of solar steam generation.[13−18] However, their performance at higher temperatures will still be limited by heat loss to the ambient through conduction, convection, and radiation. Silica aerogels, on the other hand, have been long thought to be a potential substitute for vacuum enclosures and spectrally selective surfaces in high-performance solar thermal collectors. However, high optical loss due to scattering severely offsets their thermal insulation benefits. Consequently, previous works have been limited to low-temperature operation, and it has been shown that using state-of-the-art silica aerogels is insufficient for intermediate temperature operation under one sun.[19−21]

In this work, we demonstrate an aerogel-based solar thermal receiver capable of reaching stagnation temperatures over 265 °C under unconcentrated solar flux (1 kW/m^2) at typical ambient conditions outdoors. The device consists of a blackbody absorber covered by an optimized low-scattering silica aerogel monolith as the greenhouse cavity to transmit sunlight and suppress conduction, convection, and radiation heat losses simultaneously (Figure 1a). The nanostructure of the optimized aerogel is tailored to maximize its optical transparency while maintaining its ultralow thermal conductivity. The presence of aerogel eliminates the need for a spectrally selective surface and vacuum enclosure. With both theoretical modeling and experimental investigations, we show that the receiver can be optimized to achieve over 50% efficiency at 200 °C, making it versatile for a variety of applications such as industrial process heat, solar fuel production, desalination, and solar cooling.

RESULTS AND DISCUSSION

Concept of Greenhouse Selectivity. To illustrate the potential of using the greenhouse effect for solar thermal energy conversion, we first consider the performance of an ideal greenhouse medium covering a blackbody solar absorber. The greenhouse medium provides effective spectral selectivity to a blackbody absorber by lowering its emitting temperature while keeping its high solar absorptance—a concept we describe as

DOI: 10.1021/acsnano.9b02976
ACS Nano XXXX, XXX, XXX−XXX

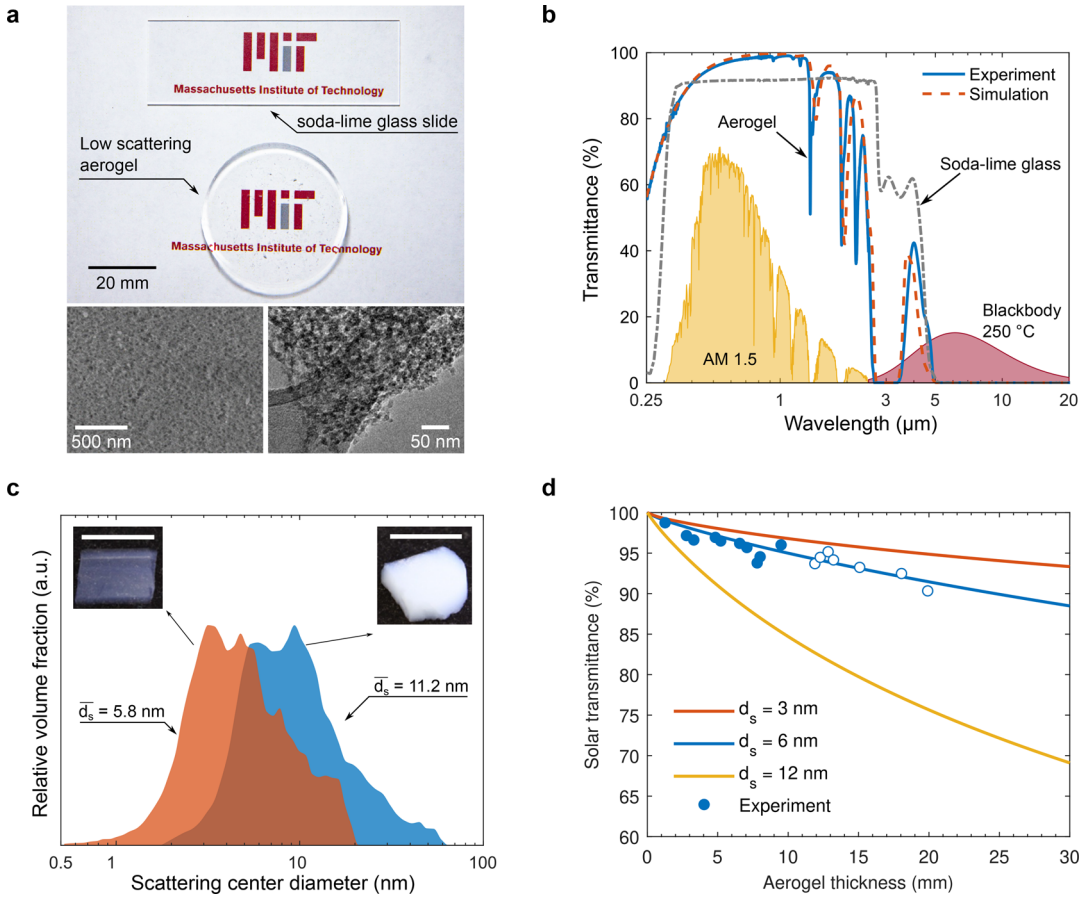

Figure 2. Low-scattering aerogel properties as a greenhouse medium. (a) Top: image of a low-scattering aerogel sample (thickness: 5 mm) and a soda-lime glass slide (thickness: 1 mm) on a piece of paper with the MIT logo (Logo printed with permission from Massachusetts Institute of Technology; Copyright 2019 Massachusetts Institute of Technology). Bottom: SEM (left) and TEM (right) images of the aerogel sample. (b) Direct-hemispherical transmittance spectrum of an 8 mm thick aerogel sample measured by a UV−vis−NIR spectrophotometer and an FTIR spectrometer. Simulation results are based on mean scattering center diameter d_s = 6.5 nm. Transmittance of the soda-lime glass slide is shown for comparison. Sharp peaks in the aerogel spectrum between 1 and 3 μm originate from absorption by water molecules and silanol groups present on the surface of silica particles. (c) Scattering center diameter d_s distribution from SAXS measurements on an optimized sample (red) and an unoptimized sample (blue). Insets: images of the two samples taken against a dark background to show the scattering effect (scale bar = 2 cm). (d) Solar-weighted transmittance as a function aerogel thickness. The lines are model results for d_s = 3, 6, 12 nm and the markers are measurements. Filled markers: single sample; Open markers: stack of two samples. The additional interface introduced by stacking two samples does not introduce a noticeable deviation from the model because of the aerogel's low refractive index.

"greenhouse selectivity". Spectral selectivity has been widely used in high-performance solar absorbers to enhance solar-to-thermal conversion efficiency by selectively absorbing solar radiation (high solar absorptance) and suppressing thermal emission[22] (low thermal emittance). To date, spectral selectivity has been realized by various surface engineering approaches, such as multilayer metal-dielectric stacks,[23] cermets,[24] and photonic crystals.[25] In our case, the greenhouse effect achieves spectral selectivity by a volumetric approach. Within the medium, solar radiation can propagate and reach the absorber while thermal emission from the absorber is significantly impeded by frequent absorption and re-emission as it passes through the medium. The frequent extinctions of thermal radiation create a thermal barrier and lower the temperature exposed to the environment. Since radiation becomes the major heat transfer mechanism at elevated temperatures, the greenhouse medium can significantly reduce the overall heat loss of a blackbody absorber.

The ideal optical properties of a greenhouse medium are depicted by a two-band model of extinction coefficient β with a cutoff wavelength around 2.5 μm (Figure 1b). To quantify the strength of greenhouse effect, we define greenhouse selectivity γ as the ratio of the extinction coefficient in the thermal band (>2.5 μm) β_{thermal} over that in the solar band (0.3−2.5 μm) β_{solar}:

$$\gamma = \frac{\beta_{\text{thermal}}}{\beta_{\text{solar}}} \tag{1}$$

with $\gamma > 1$, photons in the thermal band are extinguished more frequently than photons in the solar band, and the medium is therefore considered to have a greenhouse effect. The greenhouse selectivity introduced here can serve as a material-level figure-of-merit to help identify new greenhouse materials for solar thermal systems. On the basis of the greenhouse selectivity, the effective absorptance α and emittance ε of a greenhouse enhanced blackbody absorber (Figure 1c, inset) are

$$\alpha = \frac{q_{\text{abs}}}{q_{\text{solar}}} = \alpha_{\text{bb}} \cdot \tau_{\text{gh}} \approx e^{-\beta_{\text{solar}} L} \tag{2}$$

$$\varepsilon = \frac{q_{\text{thermal}}}{\varepsilon_{\text{bb}} \sigma (T_{\text{abs}}^4 - T_{\infty}^4)} \approx \frac{1}{{}^3/_4 \beta_{\text{thermal}} L + 1} \tag{3}$$

DOI: 10.1021/acsnano.9b02976
ACS Nano XXXX, XXX, XXX−XXX

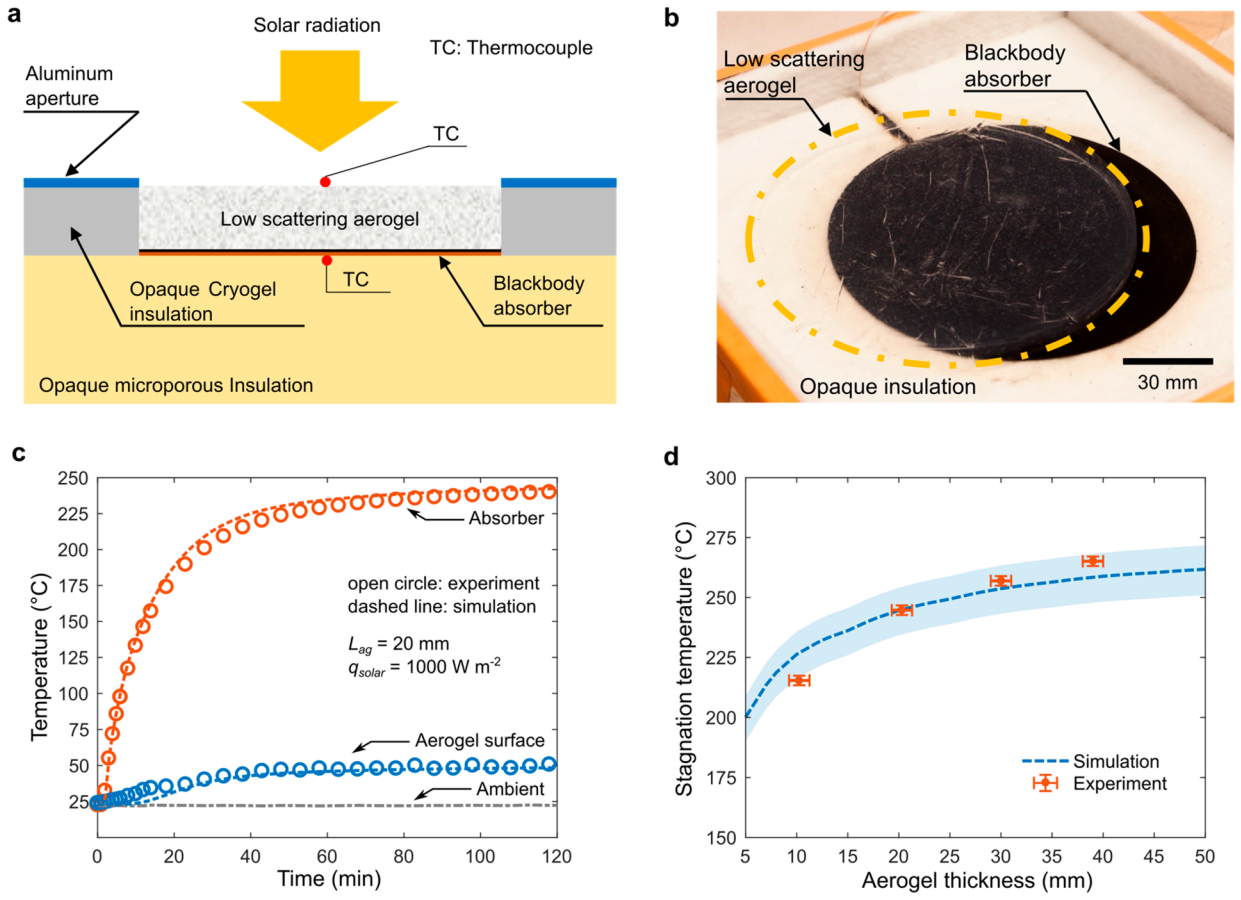

Figure 3. Aerogel enhanced solar receiver. (a) Schematic of the receiver. The black painted copper sheet serves as a blackbody absorber. Heat losses from the back of the absorber and side of the aerogel are suppressed by commercially available microporous insulation. The aerogel layer consists of one or multiple monolithic aerogel disks. (b) A close-up view of the receiver with one 10 mm thick aerogel disk (side insulation not shown). (c) Temperature response of the absorber and the aerogel surface under one sun illumination. Solar radiation was introduced at $t = 0$. The aerogel surface temperature is measured by a thermocouple shielded from solar radiation and in contact with the exposed aerogel surface. The aerogel surface temperature is significantly lower than the absorber temperature, indicating effective spatial decoupling of solar absorption (at the absorber) and thermal losses (at the aerogel surface). (d) Stagnation temperature as a function of aerogel layer thickness. The stagnation temperature first increases with aerogel thickness. As the aerogel layer thickness is increased further (beyond the values shown in the plot), the stagnation temperature will eventually reach a maximum and then decrease with aerogel thickness due to greater optical and side losses. The shaded area representing the simulation results is based on the upper (1050 W/m^2) and lower bound (950 W/m^2) of the solar simulator output flux.

respectively. Here, q_{abs}, q_{solar} are the absorbed and incident solar flux, α_{bb}, ε_{bb} are the absorptance and emittance of the blackbody absorber (equal to unity), L is the thickness of the greenhouse medium, τ_{gh} is the solar-weighted transmittance of the greenhouse medium, $q_{thermal}$ is the total heat loss from the absorber to the environment, and T_{abs} and T_{∞} are the absorber and ambient temperatures, respectively. In Figure 1c, α and ε are plotted as a function of γ, where $\gamma = 1$ represents a nongreenhouse medium with a unity optical depth ($\beta L = 1$) across the relevant wavelengths. The effective emittance decreases while the solar absorptance increases with increasing γ. When γ is greater than 300, a greenhouse enhanced blackbody absorber outperforms a typical selective surface ($\alpha \sim 0.9$, $\varepsilon \sim 0.1$). Since the greenhouse medium spatially decouples the solar absorption and suppression of thermal emission, it is a versatile approach to provide additional spectral selectivity to almost any solar absorber material[26,27] and configuration.[28−32]

In summary, an effective greenhouse medium should satisfy: (1) High greenhouse selectivity ($\gamma \gg 1$); (2) Negligible heat transfer by conduction and convection (Supplementary Note 1); (3) Thermal stability at elevated temperatures. While each individual property is not rare in common materials, their combination sets a stringent requirement. We demonstrate an optimized silica aerogel that we have tailored to possess all three desired properties to serve as an effective greenhouse medium.

Low-Scattering, Highly Transparent Aerogel. Silica aerogels are well-known as superinsulating materials due to their nanoporous structure, which simultaneously suppresses solid conduction and gas phase convection.[33] Their radiative extinction in the thermal band (2.5 μm−25 μm) is dominated by strong absorption similar to glass. These properties make silica aerogel a promising candidate as a greenhouse medium. However, unlike glass, silica aerogels typically scatter electromagnetic radiation in the visible and ultraviolet wavelengths due to scattering centers formed by silica particles and pores. The scattering behavior increases the extinction in the solar band and gives rise to the signature blue tint and translucent look of silica aerogels.[34] While extinction in the thermal band depends primarily on aerogel's density, scattering in the solar band strongly varies as a function of the scattering center size, d_s.[35] Through a rapid-hydrolysis−condensation procedure (details in Supplementary Note 2) and postsynthesis annealing to ensure

DOI: 10.1021/acsnano.9b02976
ACS Nano XXXX, XXX, XXX−XXX

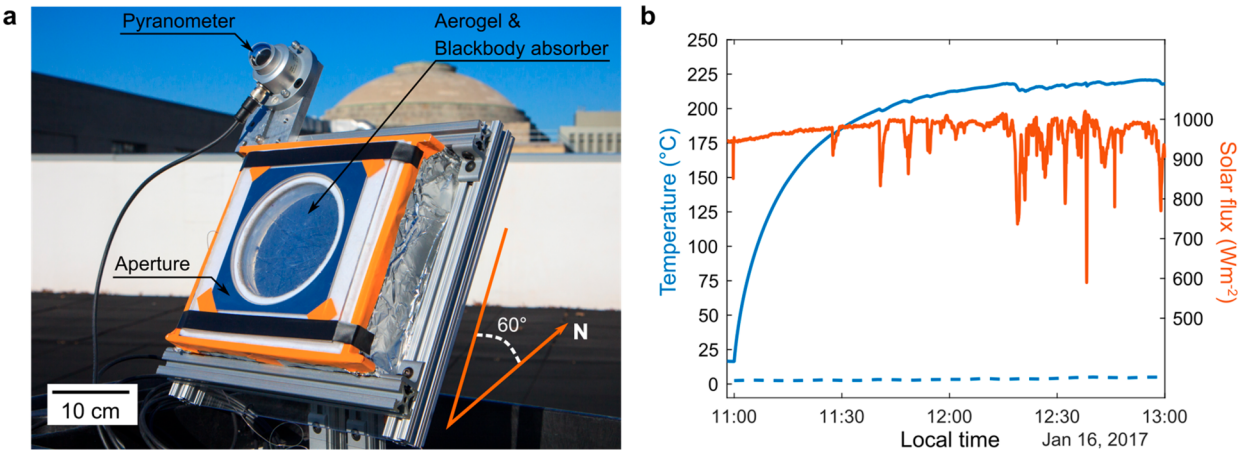

Figure 4. Aerogel receiver performance with natural sunlight on a winter day. (a) Image of the outdoor test setup on a rooftop at MIT. The receiver was tilted at a 60° angle and facing south. During the experiment, the receiver was fixed and did not track the sun. A pyranometer tilted at the same angle was used to measure the solar flux. Aerogel thickness: L_{ag} = 20 mm. (b) The absorber reached over 220 °C while the ambient temperature was close to 0 °C, demonstrating feasible operation even under winter conditions (wind speed: <2 m/s, RH: 45%, solar elevation at noon: 26.88°). The receiver maintained its temperature even when the sky became cloudy during the afternoon.

small and uniform scattering centers, we have been able to reduce the solar scattering without sacrificing strong thermal extinction.[36,37] The resultant low-scattering, highly transparent silica aerogels can transmit >95% of the sunlight at a 10 mm thickness.

Our developed aerogel (Figure 2a) is an exemplary greenhouse medium. The measured direct-hemispherical transmittance of a low-scattering aerogel sample as compared to a soda-lime glass slide, from 0.25 to 20 μm, is shown in Figure 2b. Simulation results based on the radiative transfer equation taking into account both absorption and scattering effects are also provided[38] (Supplementary Note 3). When compared to soda lime glass, the aerogel shows higher transmittance in most parts of the solar spectrum because of its low refractive index[39] (~1.05) and reduced scattering losses. In the infrared wavelengths, the aerogel has low transmittance comparable to glass. The excellent solar transparency of the aerogel originates from its nanostructure (Figure 2a bottom-pane). To quantify the scattering center size, we conducted small-angle X-ray scattering (SAXS) measurements on two representative samples (transparent and highly scattering) (Figure 2c). The scattering center diameter distributions show that the low-scattering sample has a mean scattering diameter d_s = 5.8 nm and only a slight blue tint due to weak scattering at shorter wavelengths, while the highly scattering sample has a mean scattering diameter d_s = 11.2 nm and appears completely white due to strong scattering across the visible wavelengths. The mean scattering diameter not only changes the appearance of an aerogel sample but also affects the amount of sunlight it can transmit. The simulated solar-weighted transmittance is shown as a function of aerogel thickness for d_s = 3, 6, 12 nm in Figure 2d. Experimental data on low-scattering aerogel samples were obtained by integrating the measured transmittance spectrum weighted by the AM 1.5G solar spectrum. The experimental transmittance matches the model of d_s = 6 nm which is consistent with the SAXS results. Figure 2d indicates that the scattering center size has a strong impact on the solar transmittance of an aerogel sample especially at greater thicknesses necessary for high-temperature operation. For example, at a thickness of 30 mm, the low-scattering sample (d_s = 6 nm) has a solar transmittance of 89%, compared with 69% of the highly scattering sample (d_s = 12 nm). To achieve the same level of transmittance, the thickness of the highly scattering sample needs to be reduced to 6.5 mm, which will significantly lower its thermal insulating performance. Therefore, the 50% scattering center size reduction (12 to 6 nm) is vital for efficient solar thermal conversion at higher temperatures. Even better aerogel performance can be realized if the scattering center size can be further reduced, *e.g.*, from 6 to 3 nm.

Aerogel Enhanced Solar Receiver. We constructed a solar-thermal receiver with our low-scattering aerogel in a nonevacuated enclosure (Figure 3a). The blackbody absorber is made out of a thin copper sheet (d_{abs} = 120 mm) coated by nonselective high temperature black paint (Pyromark, Tempil) with a solar absorptance α = 0.97 and thermal emittance ε = 0.85−0.9.[40] The aerogel samples were synthesized in the form of disks with the same diameter as the absorber at a thickness of L_{ag} ≈ 10 mm (Figure 3b). We created a thicker aerogel layer by stacking multiple aerogel samples. As shown in Figure 2d, the additional interfaces introduced by sample stacking show no appreciable effect on the optical transmittance. Therefore, it is possible to fabricate aerogels in standard form factors and stack multiple pieces to achieve the desired optimal performance (see details in the Model and Optimization section). Compared to conventional high performance solar thermal collectors, the proposed design is much simpler by eliminating the need for vacuum and spectrally selective surfaces.

We first investigated the performance of the aerogel solar receiver in a laboratory setup (Supplementary Note 3). An unconcentrated solar flux (1 kW/m^2) was supplied by a solar simulator in a beam-down configuration. Under illumination, the temperature of the absorber increased immediately, reached over 200 °C in 25 min, and eventually equilibrated at its steady state value, *i.e.*, the stagnation temperature (Figure 3c). The stagnation temperature is the maximum achievable temperature of a solar thermal receiver, below which the receiver can output useful thermal energy. The stagnation temperature of a nonevacuated flat plate collector with blackbody absorber is limited to 120 °C due to both radiation and convection losses.[41] With a 40 mm thick low-scattering aerogel layer, the solar receiver can reach a stagnation temperature of 265 °C (Figure 3d). This stagnation temperature is nearly 100 °C higher than

DOI: 10.1021/acsnano.9b02976
ACS Nano XXXX, XXX, XXX−XXX

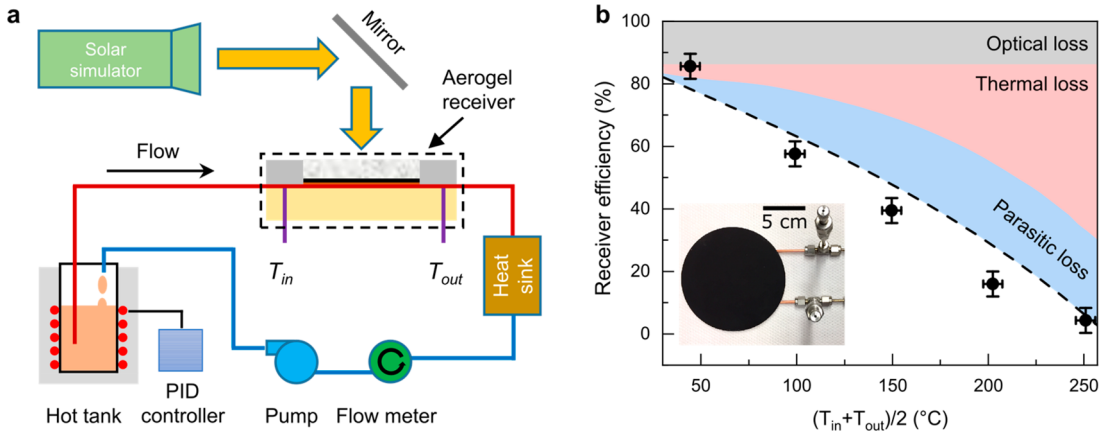

Figure 5. Aerogel receiver performance under flow conditions. (a) Schematic of the heat transfer fluid loop used for the receiver test. The fluid inlet and outlet temperatures were measured to determine the usable heat. (b) Receiver efficiency as a function of the average inlet and outlet temperatures. Each data point represents an experiment where the inlet fluid temperature was set by the hot tank and the flow rate was chosen to ensure a relatively small temperature gain (~10 °C) at the outlet, thus assuring the average of inlet and outlet temperatures is a good approximation of the absorber temperature. Experimental results with aerogel thickness L_{ag} = 40 mm are shown as black dots. The dashed line shows the modeling results for comparison. The shaded areas indicate the contribution from optical loss (aerogel transmission loss), thermal loss (from the front and back of the absorber), and parasitic loss (from the edge of the absorber and tubes). Inset: image of the absorber with fluid inlet/outlet and thermocouple fitting.

the recent prediction at the same thickness based on nonoptimal silica aerogels[21] and is comparable to the best available solar collectors with sophisticated vacuum enclosures as well as spectrally selective surfaces.[42]

To explore the receiver's performance under realistic weather conditions, we conducted an outdoor experiment on a sunny winter day (January 16, 2017) from 11 am to 1 pm at MIT campus. During the experiment, the receiver was fixed toward the south and tilted 60° from the horizontal position to maximize solar exposure (Figure 4a). After exposure to solar radiation, the absorber temperature started increasing and eventually reached over 220 °C despite the cold ambient temperature (<1 °C) and the presence of clouds in the afternoon (Figure 4b). This experiment demonstrates that the aerogel solar receiver can reach the desired intermediate temperatures even under typical winter conditions (low ambient temperature and low solar elevation angle).

In addition to measuring the stagnation temperature, we also studied the receiver performance under flow conditions. The absorber was modified by attaching a serpentine fluid channel on the back and a heat transfer fluid loop was built to circulate high-temperature heat transfer oil through the fluid channel (Figure 5a). The modified absorber was then placed in the original enclosure and covered by a 40 mm thick aerogel layer to demonstrate the highest operating temperature. During the experiment, unconcentrated solar flux was incident on the receiver and the steady-state fluid inlet and outlet temperatures were recorded to determine the heat output (details in Supplementary Note 3). The receiver efficiency was calculated as

$$\eta = \frac{\dot{m}c_p(T_{\text{out}} - T_{\text{in}})}{A_c q_{\text{solar}}} \tag{4}$$

where $\dot{m}$ is the mass flow rate, c_p is the heat capacity of the fluid, T_{in} and T_{out} are the inlet and outlet temperatures respectively, A_c is the aperture area, and q_{solar} = 1 kW/m^2 is the solar flux. The measured results are shown in Figure 5b, and are in excellent agreement with our model which considers losses in the receiver. The receiver is able to achieve 85% efficiency at 40 °C and the efficiency decreases at higher operating temperatures. Nevertheless, the receiver is able to provide heat at 250 °C, consistent with the stagnation temperature measurement. The parasitic heat losses from the edge of the absorber and tubes become significant at high temperature for the lab scale receiver. For a larger receiver, the parasitic loss could be significantly reduced and its efficiency will approach 55% and 30% at 200 and 250 °C, respectively (Figure 5b).

Model and Optimization. To better understand the experiments and explore the potential of future improvements, we carried out system modeling by tracking the energy flows within the aerogel solar receiver. The receiver gains energy by absorbing the incident solar flux transmitted through the aerogel layer. The model for this solar energy flow has been discussed in the previous section and is incorporated in the system modeling. The thermal energy flow, or heat loss, is modeled by the finite element method using COMSOL with the thermal conductivity of each receiver component as an input. The effective thermal conductivity of the aerogel is evaluated by a theoretical model considering solid and gaseous conduction, convection and thermal radiation within the aerogel[20,33,43,44] (details in Supplementary Note 4). The COMSOL thermal model is validated by heat loss measurements performed on the constructed receiver using an electrical heater as the power input instead of the solar simulator (details in Supplementary Note 4). By combining the optical model and the thermal model, our receiver model can predict the temperature of the absorber under both transient (Figure 3c) and steady state (Figure 3d) conditions.

Besides achieving high stagnation temperatures, the useful heat output of a receiver under flow conditions is another important metric. The heat output of a receiver depends on many factors, including the optical efficiency (η_{opt}), absorber efficiency (η_{abs}), and heat removal efficiency (η_{hr}).[45] For the nonconcentrating system in this study, the optical efficiency is simply the transmittance of a protective glass cover. The heat removal efficiency measures how efficiently the heat output of an absorber is transferred out, typically by a heat transfer fluid

DOI: 10.1021/acsnano.9b02976
ACS Nano XXXX, XXX, XXX−XXX

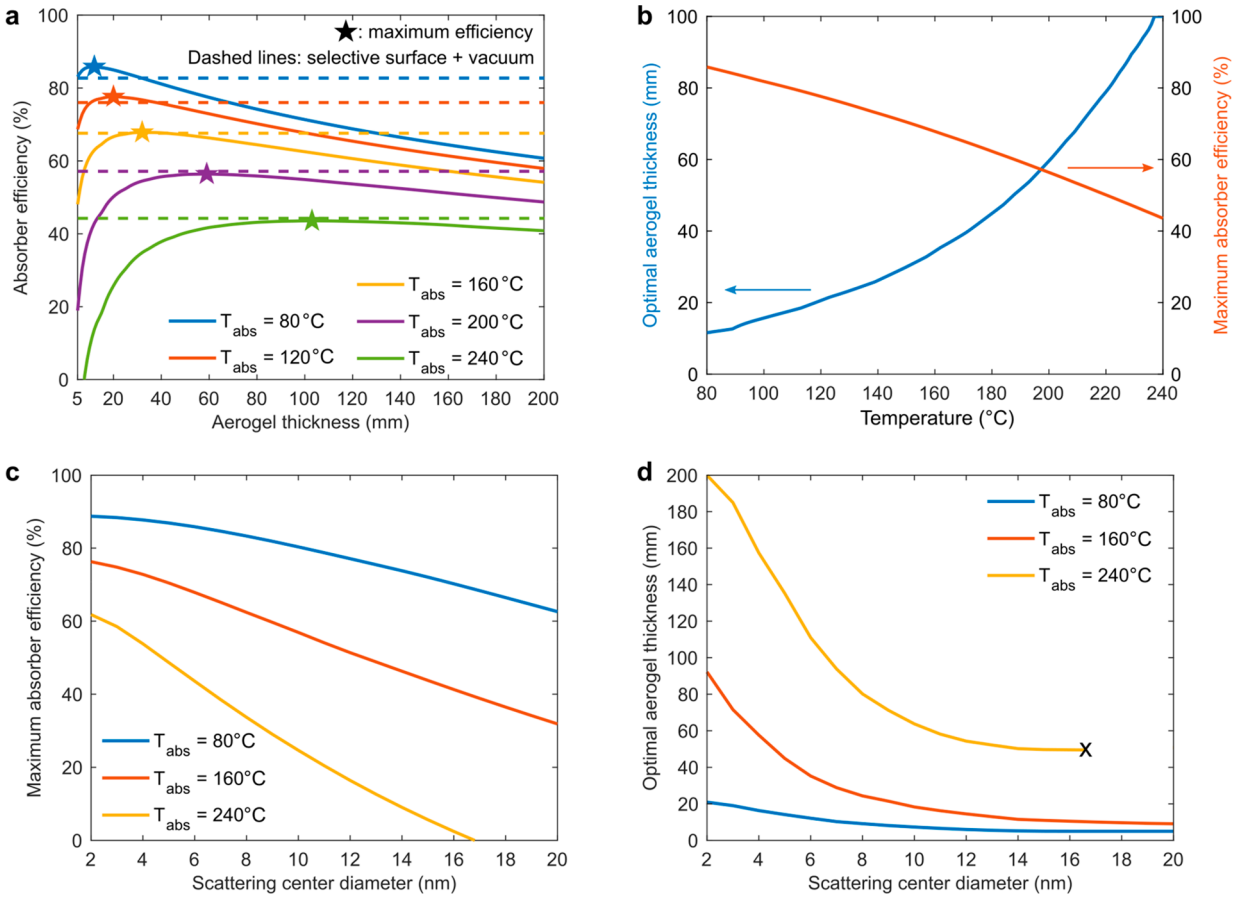

Figure 6. Aerogel blackbody absorber performance and optimization. Aerogel properties: d_s = 6 nm, density = 200 kg/m^3 unless otherwise stated. q_{sol} = 1 kW/m^2. (a) Absorber efficiency as a function of aerogel thickness for various operating temperatures. The star indicates the maximum efficiency point. The efficiency curves gradually plateau after a certain thickness. Dashed lines are efficiencies achieved by a typical selective surface in a vacuum enclosure at corresponding temperatures. (b) Optimal aerogel thickness and maximum achievable efficiency as a function of operating temperature. (c,d) Sensitivity of the maximum efficiency, and optimal aerogel thickness, to the aerogel scattering center diameter d_s. Smaller scattering center reduces the transmittance loss penalty and increases both the optimal aerogel thickness and the maximum achievable efficiency. Scattering center diameter greater than ~17 nm results in negative efficiency at 240 °C.

flowing on the backside of an absorber. The absorber efficiency describes how efficiently sunlight is converted into useful heat at the absorber. The overall solar to thermal conversion efficiency can then be expressed as the product of the subcomponent efficiencies:

$$\eta = \eta_{opt}\eta_{abs}\eta_{hr} \tag{5}$$

The modeling results of the receiver heat output are plotted in Figure 5b (details in Supplementary Note 4).

As the focus of the study is to demonstrate an absorber configuration, it is convenient to use the absorber efficiency:

$$\eta_{abs} = \alpha_{sol} - \frac{h_L(T_{abs} - T_\infty)}{\eta_{opt} q_{solar}} \tag{6}$$

where α_{sol} is the solar weighted absorptance, h_L is the linearized overall heat loss coefficient from the absorber to the ambient, including both radiation and conduction contributions within the aerogel, T_{abs} and T_∞ are the absorber and ambient temperature, η_{opt} is the glass cover transmittance, which is assumed to be unity in this analysis, q_{solar} is the solar flux (1 kW/m^2). The absorber efficiency quantifies the useful heat output from an absorber under a fixed input solar power and provides a common baseline for comparing the performance of different absorbers as it only depends on the absorber optical and thermal properties (for a full solar collector comparison, see details in Supplementary Note 4). In Figure 6a, the aerogel blackbody absorber efficiency is plotted as a function of aerogel thickness for various absorber temperatures. For each absorber temperature, an optimal thickness exists. A higher absorber temperature results in a thicker optimal aerogel because of the greater importance of minimizing heat loss. For comparison, the absorber efficiency of a typical selective surface in vacuum (solar absorptance α_{sol} = 0.9, thermal emittance ε = 0.1, parasitic loss coefficient h_c = 0.5 W/m^{2}K) is plotted as dashed lines in Figure 6a (details in Supplementary Note 4). The aerogel blackbody absorber configuration can achieve a comparable absorber performance at the optimal aerogel thickness. Figure 6b shows the optimal aerogel thickness and maximum absorber efficiency as a function of the absorber temperature. It is worth noting that this optimal thickness does not consider the aerogel cost. As shown in Figure 6a, the efficiency curve nearly plateaus after a certain thickness, especially at high temperatures. Therefore, when considering cost, the aerogel thickness can be reduced with a small efficiency penalty. As mentioned previously, the scattering center diameter d_s largely dictates the optical transparency of the aerogel. In Figure 6c, we show a sensitivity study of scattering center diameters d_s to the maximum absorber efficiency. The absorber efficiency quickly

DOI: 10.1021/acsnano.9b02976
ACS Nano XXXX, XXX, XXX−XXX

degrades with scattering center size as the solar transmittance decreases due to strong scattering (Figure 2d). In this work, the optimized aerogel has a scattering center diameter around 6 nm, much smaller than previously reported values of around 20 nm.[34] This fundamental improvement enables us to use a thicker aerogel layer to reduce the heat loss without incurring a significant optical loss[21,46] as shown in Figure 6d.

CONCLUSIONS

The integration of a low-scattering aerogel layer of reasonable thickness with nonevacuated flat plate solar collectors can boost its efficiency, especially at high temperatures (>120 °C). Although not optimal, a 20 mm aerogel layer can already achieve higher than 50% absorber efficiency for temperatures below 200 °C, which satisfies a major portion of the thermal energy demand. The ability to convert unconcentrated sunlight at this intermediate temperature without the need of costly optical and mechanical components provides an exciting pathway to promote solar thermal energy utilization.

MATERIALS AND METHODS

Aerogel Synthesis. The low-scattering silica aerogel was synthesized by sol−gel polymerization of tetramethyl orthosilicate (TMOS, 131903, Sigma-Aldrich), using an ammonia solution (NH_3, 2.0 M in Methanol, 341428, Sigma-Aldrich) as a catalyst to promote both hydrolysis and condensation reactions. TMOS was diluted by methanol (MeOH, 322415, Sigma-Aldrich) followed by addition of NH_3 and water. The mixing molar ratio of chemicals was NH_3:TMOS:water:methanol = 0.0348:1:4:6.42. Then, the solution was gelled in a disposable polystyrene container. After 2 weeks, the container was dissolved away using acetone. The mother solvent was replaced with ethanol (EtOH, 89234−848, VWR) to be prepared for critical point drying (CPD, model 931, Tousimis) as EtOH is miscible with liquid CO_2. To dry the wet gels in EtOH without cracks, it is important to dry them slowly to minimize capillary pressure during the CPD process. A bleed rate of 100 psi/h was used to decrease the CPD chamber pressure from ∼1300 psi to ambient pressure. After drying, the monolithic aerogels were annealed at 400 °C for 24 h to maximize their transmittance.

Optical Property Measurement. The direct-hemispherical transmittance of our prepared aerogel samples was measured using a UV−vis−NIR spectrophotometer (Agilent Cary 5000) with an integrating sphere (Internal DRA-2500, Agilent) and a Fourier transform infrared (FTIR) spectrometer (Nicolet 5700) with a Pike Technologies mid-IR integrating sphere. A custom-built sample holder was used to load samples into the spectrophotometer.

SAXS Measurement. SAXS was used to determine the scattering length distribution and estimate the average scattering radius size. Characterization was done on a SAXSLAB custom-built instrument using a Cu Kα X-ray source. Samples were probed at multiple points within the sample to check consistency of structure—from the center to edge. The scattering patterns were reduced and corrected using SAXSGUI software, and the mean scattering radii were estimated using MCSAS software and verified in SasView.

Solar Receiver Construction. The aerogel solar receiver enclosure was constructed using commercially available thermal insulation material (MICROSIL, Zircar Ceramic, and Cryogel, Aspen Aerogel). The substrate of the blackbody absorber used in the experiment was made out of a copper sheet (thickness = 0.45 mm) machined to the desired size by water jet (OMAX Micro jet). A K-type thermocouple (5TC-KK-K-30-36, OMEGA Engineering) was attached to the back of the absorber using a thermally conductive silver paste (High Performance Silver Paste, PELCO). An aperture made of a reflective aluminum sheet was used to reflect the solar flux incident on the inactive area of the receiver. For the flow measurement, a serpentine fluid channel (1/8-in. copper tube) was attached to the back of the absorber using the same silver paste.

Outdoor Test. The outdoor test was conducted on the rooftop of Building 1 at MIT. The solar flux was measured using a Hukseflux LP-02 thermal pyranometer. The weather data was measured by a weather station on the same rooftop.

ASSOCIATED CONTENT

Supporting Information

The Supporting Information is available free of charge on the ACS Publications website at DOI: 10.1021/acsnano.9b02976.

Details on aerogel thermal and optical model, aerogel synthesis optimization, aerogel longevity study, and aerogel enhanced solar receiver experiment and model (PDF)

AUTHOR INFORMATION

Corresponding Authors

*E-mail: gchen2@mit.edu.
*E-mail: enwang@mit.edu.

ORCID

Lin Zhao: 0000-0002-8865-859X
Evelyn N. Wang: 0000-0001-7045-1200

Present Addresses

[†]Chemical Engineering Department, University of Tennessee at Chattanooga, 615 McCallie Avenue, Chattanooga, Tennessee 37403, United States.
[‡]Department of Mechanical Engineering, York University, 4700 Keele Street, Toronto, Ontario M3J 1P3, Canada.

Author Contributions

L.Z. designed and conducted the experiments with extensive contributions from all authors: S.Y. (aerogel synthesis), E.S. and B.B. (aerogel characterization), B.B., L.A.W., and T.A.C. (experimental setup). L.Z. and B.B. conducted the theoretical studies. L.Z. wrote the paper with input from all authors. G.C. and E.N.W supervised and guided the overall research.

Notes

The authors declare no competing financial interest.

ACKNOWLEDGMENTS

The authors thank G. Ni and D. Bierman for advice and experimental help. This work was mainly supported by the ARPA-E FOCUS program under award number DE-AR0000471 (aerogel fabrication, aerogel thermal characterization, receiver modeling, and receiver experiments). This work made use of experiment facilities from the Solid-State Solar Thermal Energy Conversion (S^3TEC) Center, an Energy Frontier Research Center funded by the US Department of Energy, Office of Science, Basic Energy Sciences under Award Number DE-FG02-09ER46577 (aerogel optical characterization). This work benefitted from SasView software, originally developed by the DANSE project under NSF Award DMR-052054 (SAXS measurements).

REFERENCES

(1) *Climate Change 2014: Synthesis Report*; Intergovernmental Panel on Climate Change (IPCC): Geneva, Switzerland, 2014.
(2) Weinstein, L. A.; Loomis, J.; Bhatia, B.; Bierman, D. M.; Wang, E. N.; Chen, G. Concentrating Solar Power. *Chem. Rev.* **2015**, *115*, 12797−12838.
(3) Kurup, P.; Turchi, C. *Initial Investigation into the Potential of CSP Industrial Process Heat for the Southwest United States*; National Renewable Energy Laboratory (NREL): Golden, CO, 2015.

DOI: 10.1021/acsnano.9b02976
ACS Nano XXXX, XXX, XXX−XXX

(4) *Electric Power Monthly: With Data for September 2016*; U.S. Energy Information Administration (EIA): Washington, D.C., 2016.
(5) Keith, L.; Stein, W. *Concentrating Solar Power Technology*; Woodhead Publishing: Cambridge, 2012; pp 6−13.
(6) *Technology Roadmap Solar Thermal Electricity*; International Energy Agency: Paris, France, 2014.
(7) *Middle East and North Africa Region Assessment of the Local Manufacturing Potential for Concentrated Solar Power (CSP) Projects*; World Bank: Washington, D.C., 2011.
(8) Zimmerman, R.; Morrison, G.; Rosengarten, G. A Solar Powered Microreactor for Hydrogen Production by Methanol Reforming. ASME. Energy Sustainability, In *ASME 2008 2nd Int. Conf. Energy Sustain.*; ASME, 2008; Vol. *2*, pp 391−396.
(9) Real, D.; Johnston, R.; Lauer, J.; Schicho, A.; Hotz, N. Novel Non-Concentrating Solar Collector for Intermediate-Temperature Energy Capture. *Sol. Energy* **2014**, *108*, 421−431.
(10) Föste, S.; Giovannetti, F.; Ehrmann, N.; Rockendorf, G. Performance and Reliability of a High Efficiency Flat Plate Collector - Final Results on Prototypes. *Energy Procedia* **2014**, *48*, 48−57.
(11) Beikircher, T.; Möckl, M.; Osgyan, P.; Streib, G. Advanced Solar Flat Plate Collectors with Full Area Absorber, Front Side Film and Rear Side Vacuum Super Insulation. *Sol. Energy Mater. Sol. Cells* **2015**, *141*, 398−406.
(12) Thomas, N. H.; Chen, Z.; Fan, S.; Minnich, A. J. Semiconductor-Based Multilayer Selective Solar Absorber for Unconcentrated Solar Thermal Energy Conversion. *Sci. Rep.* **2017**, *7*, 5362.
(13) Shao, Y.; Jiang, Z.; Zhang, Y.; Wang, T.; Zhao, P.; Zhang, Z.; Yuan, J.; Wang, H. All-Poly(Ionic Liquid) Membrane-Derived Porous Carbon Membranes: Scalable Synthesis and Application for Photothermal Conversion in Seawater Desalination. *ACS Nano* **2018**, *12*, 11704−11710.
(14) Yang, Y.; Zhao, R.; Zhang, T.; Zhao, K.; Xiao, P.; Ma, Y.; Ajayan, P. M.; Shi, G.; Chen, Y. Graphene-Based Standalone Solar Energy Converter for Water Desalination and Purification. *ACS Nano* **2018**, *12*, 829−835.
(15) Yang, J.; Pang, Y.; Huang, W.; Shaw, S. K.; Schiffbauer, J.; Pillers, M. A.; Mu, X.; Luo, S.; Zhang, T.; Huang, Y.; Li, G.; Ptasinska, S.; Lieberman, M.; Luo, T. Functionalized Graphene Enables Highly Efficient Solar Thermal Steam Generation. *ACS Nano* **2017**, *11*, 5510−5518.
(16) Li, R.; Zhang, L.; Shi, L.; Wang, P. MXene Ti3C2: An Effective 2D Light-to-Heat Conversion Material. *ACS Nano* **2017**, *11*, 3752−3759.
(17) Zhang, P.; Li, J.; Lv, L.; Zhao, Y.; Qu, L. Vertically Aligned Graphene Sheets Membrane for Highly Efficient Solar Thermal Generation of Clean Water. *ACS Nano* **2017**, *11*, 5087−5093.
(18) Neumann, O.; Urban, A. S.; Day, J.; Lal, S.; Nordlander, P.; Halas, N. J. Solar Vapor Generation Enabled by Nanoparticles. *ACS Nano* **2013**, *7*, 42−49.
(19) Svendsen, S. Solar Collector with Monolithic Silica Aerogel. *J. Non-Cryst. Solids* **1992**, *145*, 240−243.
(20) Nordgaard, A.; Beckman, W. A. Modelling of Flat-Plate Collectors Based on Monolithic Silica Aerogel. *Sol. Energy* **1992**, *49*, 387−402.
(21) Günay, A. A.; Kim, H.; Nagarajan, N.; Lopez, M.; Kantharaj, R.; Alsaati, A.; Marconnet, A.; Lenert, A.; Miljkovic, N. Optically Transparent Thermally Insulating Silica Aerogels for Solar Thermal Insulation. *ACS Appl. Mater. Interfaces* **2018**, *10*, 12603−12611.
(22) Bermel, P.; Lee, J.; Joannopoulos, J.; Celanovic, I.; Soljacic, M. Selective Solar Absorbers. *Annu. Rev. Heat Transfer* **2012**, *15*, 231−254.
(23) Narayanaswamy, A.; Chen, G. Thermal Emission Control with One-Dimensional Metallodielectric Photonic Crystals. *Phys. Rev. B: Condens. Matter Mater. Phys.* **2004**, *70*, 125101.
(24) Cao, F.; McEnaney, K.; Chen, G.; Ren, Z. A Review of Cermet-Based Spectrally Selective Solar Absorbers. *Energy Environ. Sci.* **2014**, *7*, 1615−1627.
(25) Chou, J. B.; Yeng, Y. X.; Lee, Y. E.; Lenert, A.; Rinnerbauer, V.; Celanovic, I.; Soljačić, M.; Fang, N. X.; Wang, E. N.; Kim, S. G. Enabling Ideal Selective Solar Absorption with 2D Metallic Dielectric Photonic Crystals. *Adv. Mater.* **2014**, *26*, 8041−8045.
(26) Mizuno, K.; Ishii, J.; Kishida, H.; Hayamizu, Y.; Yasuda, S.; Futaba, D. N.; Yumura, M.; Hata, K. A Black Body Absorber from Vertically Aligned Single-Walled Carbon Nanotubes. *Proc. Natl. Acad. Sci. U. S. A.* **2009**, *106*, 6044−6047.
(27) Zhou, L.; Tan, Y.; Ji, D.; Zhu, B.; Zhang, P.; Xu, J.; Gan, Q.; Yu, Z.; Zhu, J. Self-Assembly of Highly Efficient, Broadband Plasmonic Absorbers for Solar Steam Generation. *Sci. Adv.* **2016**, *2*, No. e1501227.
(28) Lenert, A.; Wang, E. N. Optimization of Nanofluid Volumetric Receivers for Solar Thermal Energy Conversion. *Sol. Energy* **2012**, *86*, 253−265.
(29) Weinstein, L.; Kraemer, D.; McEnaney, K.; Chen, G. Optical Cavity for Improved Performance of Solar Receivers in Solar-Thermal Systems. *Sol. Energy* **2014**, *108*, 69−79.
(30) Weinstein, L. A.; McEnaney, K.; Strobach, E.; Yang, S.; Bhatia, B.; Zhao, L.; Huang, Y.; Loomis, J.; Cao, F.; Boriskina, S. V.; Ren, Z.; Wang, E. N.; Chen, G. A Hybrid Electric and Thermal Solar Receiver. *Joule* **2018**, *2*, 962−975.
(31) Ni, G.; Li, G.; Boriskina, S. V. V.; Li, H.; Yang, W.; Zhang, T. J.; Chen, G. Steam Generation under One Sun Enabled by a Floating Structure with Thermal Concentration. *Nat. Energy* **2016**, *1*, 16126.
(32) Kim, H.; Rao, S. R.; Kapustin, E. A.; Zhao, L.; Yang, S.; Yaghi, O. M.; Wang, E. N. Adsorption-Based Atmospheric Water Harvesting Device for Arid Climates. *Nat. Commun.* **2018**, *9*, 1191.
(33) Hrubesh, L. W.; Pekala, R. W. Thermal Properties of Organic and Inorganic Aerogels. *J. Mater. Res.* **1994**, *9*, 731−738.
(34) Pajonk, G. M. Transparent Silica Aerogels. *J. Non-Cryst. Solids* **1998**, *225*, 307−314.
(35) Emmerling, A.; Petricevic, R.; Beck, A.; Wang, P.; Scheller, H.; Fricke, J. Relationship between Optical Transparency and Nanostructural Features of Silica Aerogels. *J. Non-Cryst. Solids* **1995**, *185*, 240−248.
(36) Strobach, E.; Bhatia, B.; Yang, S.; Zhao, L.; Wang, E. N. High Temperature Annealing for Structural Optimization of Silica Aerogels in Solar Thermal Applications. *J. Non-Cryst. Solids* **2017**, *462*, 72−77.
(37) Zhao, L.; Strobach, E.; Bhatia, B.; Yang, S.; Leroy, A.; Zhang, L.; Wang, E. N. Theoretical and Experimental Investigation of Haze in Transparent Aerogels. *Opt. Express* **2019**, *27*, A39−A50.
(38) Zhao, L.; Yang, S.; Bhatia, B.; Strobach, E.; Wang, E. N. Modeling Silica Aerogel Optical Performance by Determining Its Radiative Properties. *AIP Adv.* **2016**, *6*, 025123.
(39) Buzykaev, A. R.; Danilyuk, A. F.; Ganzhur, S. F.; Kravchenko, E. A.; Onuchin, A. P. Measurement of Optical Parameters of Aerogel. *Nucl. Instrum. Methods Phys. Res., Sect. A* **1999**, *433*, 396−400.
(40) Ho, C. K.; Mahoney, A. R.; Ambrosini, A.; Bencomo, M.; Hall, A.; Lambert, T. N. Characterization of Pyromark 2500 Paint for High-Temperature Solar Receivers. *J. Sol. Energy Eng.* **2014**, *136*, 014502.
(41) Harrison, S.; Cruickshank, C. A. A Review of Strategies for the Control of High Temperature Stagnation in Solar Collectors and Systems. *Energy Procedia* **2012**, *30*, 793−804.
(42) Zimmerman, R. E. Novel Micro Solar Collector for Portable Hydrogen Production. Ph.D. Thesis, The University of New South Wales, 2011.
(43) Heinemann, U.; Caps, R.; Fricke, J. Radiation-Conduction Interaction : An Investigation on Silica Aerogels. *Int. J. Heat Mass Transfer* **1996**, *39*, 2115−2130.
(44) McEnaney, K.; Weinstein, L.; Kraemer, D.; Ghasemi, H.; Chen, G. Aerogel-Based Solar Thermal Receivers. *Nano Energy* **2017**, *40*, 180−186.
(45) Duffie, J. A.; Beckman, W. A. *Solar Engineering of Thermal Processes*; John Wiley & Sons: Hoboken, NJ, 2013; pp 262−266.
(46) Duer, K.; Svendsen, S. Monolithic Silica Aerogel in Super-insulating Glazings. *Sol. Energy* **1998**, *63*, 259−267.

DOI: 10.1021/acsnano.9b02976
ACS Nano XXXX, XXX, XXX−XXX